Renewal of the Holocrine Meibomian Glands by Label-Retaining, Unipotent Epithelial Progenitors

Geraint J. Parfitt,[1] Phillip N. Lewis,[2] Robert D. Young,[2] Alex Richardson,[3] J. Guy Lyons,[4] Nick Di Girolamo,[3] and James V. Jester[1,*]

[1]The Gavin Herbert Eye Institute, University of California Irvine, 843 Health Sciences Road, Irvine, CA 92697-4390, USA
[2]The School of Optometry & Vision Sciences, Cardiff University, Maindy Road, Cardiff CF24 4HQ, UK
[3]School of Medical Sciences, University of New South Wales, Sydney, NSW 2052, Australia
[4]Centenary Institute and Discipline of Dermatology, Bosch Institute, Sydney Medical School, University of Sydney, Sydney, NSW 2050, Australia
*Correspondence: jjester@uci.edu
http://dx.doi.org/10.1016/j.stemcr.2016.07.010

SUMMARY

The meibomian and sebaceous glands secrete lipids to prevent desiccation of the ocular surface and skin, respectively. Precisely how these holocrine tissues regenerate is not well understood. To address this, we characterized keratin 5[+] (K5) label-retaining cells (LRCs) and the lineage tracing of keratin 14 (K14) progenitors in mouse meibomian glands. Using the tet-off H2B-GFP/K5tTA mouse, H2B-GFP fluorescence dilutes 2-fold with every division in K5[+] cell nuclei after doxycycline administration. In 3D reconstructions generated over a >28-day doxycycline chase, we observed LRCs at the acinus entrance where K6[+] ductal epithelium terminates. For lineage tracing, K14CreER[T2]-Confetti mice were injected intraperitoneally with tamoxifen and euthanized at 23 and 59 weeks later. Meibomian gland acini in these mice were either monochromatic or dual-colored, whereas the duct exhibited multiple colors. In conclusion, LRCs are likely to direct meibomian gland turnover and may exist as two distinct unipotent progenitors that renew ductal and acinar tissue separately.

INTRODUCTION

The holocrine meibomian glands are embedded in the eyelid tarsal plate and secrete lipid (meibum) onto the ocular surface tear film to reduce aqueous tear evaporation and evaporative stress. Meibomian gland atrophy and hyposecretion of meibum has been linked to the development of evaporative dry eye, which is a common age-related, ocular surface disorder that can seriously impair vision (Horwath-Winter et al., 2003; Lemp et al., 2012). Meibum is synthesized by enlarged, terminally differentiated meibocytes that form the acini of the meibomian gland, and is delivered through the central duct to the mucocutaneous junction of the eyelid margin. The mechanism that explains how the acinar and ductal epithelia renew throughout life has not been well described, and there is only limited information about a putative meibomian gland stem cell population (Knop et al., 2011; Olami et al., 2001; Parfitt et al., 2015).

Meibomian glands share similar characteristics with the sebum-producing sebaceous glands adjoined to hair follicles, as they are developmentally similar skin appendages with comparable keratin-expression profiles (Knop et al., 2011). For example, all basal epithelial cells of the developing (Call et al., 2016) and adult mouse meibomian gland (Parfitt et al., 2013) exhibit type I (acidic) keratin 14 (K14), which heterodimerizes with type II (basic) keratin 5 (K5) to form the intermediate filaments that constitute their cytoskeleton. As in sebaceous glands, basal acinar cells of the meibomian gland differentiate and move centripetally

toward the center of an acinus before lipogenesis and holocrine secretion. These terminally differentiated meibocytes synthesize and accumulate lipid, express high levels of peroxisome proliferator-activated receptor gamma (PPAR-γ), and undergo cell degeneration and disintegration of the cell membrane and nuclear material (pyknosis). This lifelong differentiation and destruction of acinar cells requires continual turnover of the basal layer and suggests the presence of a proximal stem cell reservoir to provide long-term self-renewal, as is the case with other epithelial tissues such as the hair follicle (Cotsarelis et al., 1990; Tumbar et al., 2004), corneal epithelium (Cotsarelis et al., 1989; Di Girolamo et al., 2015; Stepp and Zieske, 2005), and intestine (Barker et al., 2007; Pinto and Clevers, 2005). Therefore, characterizing meibomian gland progenitors may provide important insights into holocrine tissue regeneration and dysfunction, as it has recently been shown that the meibomian gland hyperproliferates in response to environmental evaporative stress (Suhalim et al., 2014), while aging in both humans and mice results in hypoproliferation and atrophic changes (Nien et al., 2009, 2011; Parfitt et al., 2013).

Adult stem cells are defined as undifferentiated, multipotent progenitor cells with the capability to both self-renew and generate differentiated progeny throughout the lifetime of an organism (Alonso and Fuchs, 2003; Blanpain and Fuchs, 2006; Fuchs and Segre, 2000; Lavker and Sun, 1983; Lavker et al., 2004; Sun et al., 1991; Tumbar et al., 2004). Through asymmetrical division, they are able to reproduce an identical daughter cell and a transiently

amplifying cell, which rapidly proliferates to meet the turn-over requirements of the tissue. Adult stem cells are considered to be quiescent, or divide infrequently, but rapidly proliferate when placed in cell culture (Fuchs and Horsley, 2011; Stepp and Zieske, 2005). Slow-cycling, putative adult stem cells have been localized in several different ocular epithelia, including the conjunctiva (Chen et al., 2003; Nadri et al., 2008; Nagasaki and Zhao, 2005; Su et al., 2011; Vascotto and Griffith, 2006), corneal limbus (Cotsarelis et al., 1989; Di Girolamo et al., 2015; Parfitt et al., 2015), and lacrimal gland (You et al., 2011). The characteristics of label-retaining cells (LRCs) or a stem cell "niche" in the meibomian gland is not well characterized. However, recent evidence using the H2B-GFP/K5tTA mouse suggests that the terminal ends of the ductal epithelium are potential sites of adult progenitors or stem cells of the meibomian gland (Parfitt et al., 2015), rather than the central duct or peripheral acinar cells as has previously been suggested (Lavker, 2003; Olami et al., 2001).

Generation of the H2B-GFP/K5tTA bigenic mouse (Tumbar et al., 2004) enabled the visualization of slow-cycling LRCs in mouse epidermis using the "tet-off" model and pulse-chase labeling with doxycycline. This model uses the K5 promoter-driven transactivator (tTA) protein that binds to a tetracycline-responsive element and activates histone H2B-GFP fusion transgene expression in the absence of doxycycline. When doxycycline is present in the mouse's diet, H2B-GFP expression is switched off and GFP label will be diluted 2-fold with every division in K5$^+$ epithelial cells. Therefore, only cells that divide infrequently will retain GFP fluorescence after multiple rounds of cell division. This mouse is invaluable for characterizing adult epithelial stem cells as the toxicity of radiolabeling and bromodeoxyuridine (usual reagents used to mark LRCs) means that the slowest cycling cells are unlabeled with a restricted pulse phase (Duque and Rakic, 2011). Due to the rarity of adult stem cells in a tissue such as the meibomian gland, imaging single-cell fluorescence and lineage tracing can be difficult and prone to sampling error in 2D sections, which are typically cut at 5 μm or more in frozen and paraffin sections. To address these problems, we have used immunofluorescence tomography to 3D reconstruct and quantify LRCs with high axial resolution (0.4 μm × 0.4 μm × 2 μm) in a large tissue volume (mm^3) (Parfitt et al., 2012). We have previously applied immunofluorescence tomography to the mouse meibomian gland to characterize keratinization in the aging meibomian gland (Parfitt et al., 2013), and to quantify the label-retaining cells of the murine corneal epithelium, as well as the meibomian and sebaceous glands, whereby we quantified the total number of LRCs per meibomian gland at 28-day (25 ± 4), 42-day (12 ± 2), and 56-day (9 ± 3) doxycycline chase (Parfitt et al., 2015).

In this study, immunofluorescence tomography was used to 3D characterize K6 expression of LRCs, as well as the lineage-tracing signals of K14 progenitors in the mouse meibomian gland. For lineage tracing of K14, The K14CreER^{T2}-Confetti transgenic mouse harboring the Brainbow 2.1 cassette has previously been used to study epidermal regeneration (Rinkevich et al., 2011) and limbal epithelial stem cells (Amitai-Lange et al., 2015; Di Girolamo et al., 2015), and was used here to investigate the turnover of meibomian glands. We observed LRCs located at the terminal ends of the K6$^+$ ductal epithelium where it meets an acinus. Furthermore, we observed a variation in label retention of meibomian gland LRCs, which implies that the cell-cycle rate is not uniform among slow-cycling epithelial cells. Finally, we hypothesize that unipotent progenitors separately give rise to the ductal and acinar components of the meibomian gland, a finding supported by our lineage-tracing data whereby acini are exclusively composed of a single lineage that does not extend into the ductal epithelium or to another acinus.

RESULTS

Short- and Long-Term Doxycycline Chase of the H2B-GFP/K5tTA Mouse to Characterize Label Dilution and LRCs in the Meibomian Gland

Prior to quantifying LRCs over long-term (26- to 56-day) chase, we evaluated the short-term (<16-day) proliferation status of the meibomian gland over the course of a 16-day chase in 10-μm cryosections (Figure 1). At postnatal day 28 following continued labeling from postnatal day 0, all epithelial cells in the meibomian gland exhibited nuclear GFP (Figure 1A), as demonstrated by a consistent fluorescence intensity across the gland in a pixel heatmap (Figure 1E). After 9-day doxycycline chase there was considerable variation in label dilution and cell-cycle rate between acini and the central duct, as some basal acinar cells were observed to be diluted of GFP (Figures 1B and 1F, red arrowheads). At 13-day doxycycline chase (Figures 1C and 1G), some acinar cells were completely diluted (red arrowhead) while others were only partially diluted (white arrowhead), implying that acinar turnover is not uniform, or synchronous across the meibomian gland. Moreover, the ductal epithelium remained largely GFP$^+$ at the 13- and 16-day time points, while the majority of acini were diluted of GFP signal at 16 days post doxycycline (Figures 1D and 1H). This short-term chase experiment illustrates the difference in cell-turnover rates between each acinus, and between the acini and ductal epithelium of the meibomian gland.

From the 3D reconstructions generated by immunofluorescence tomography, a low quantity of slow-cycling,
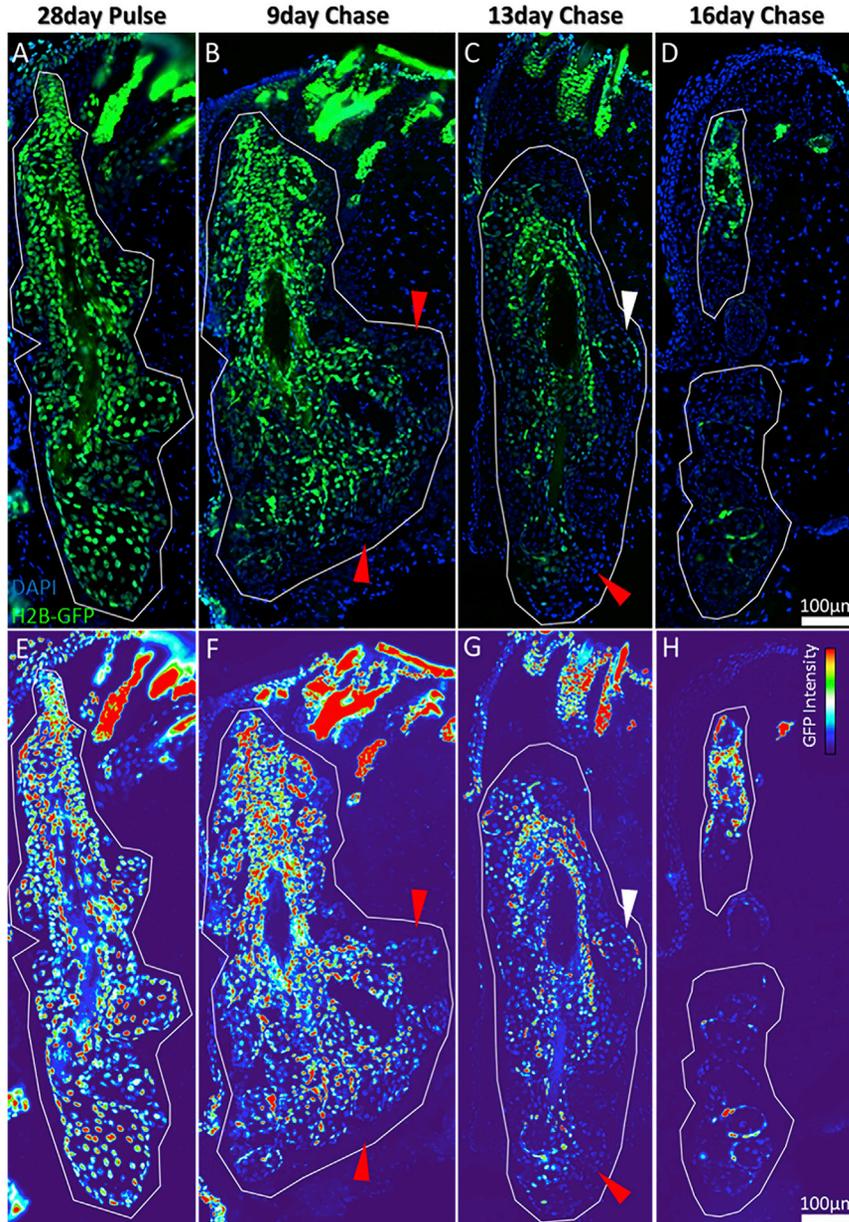
Figure 1. Short-Term Doxycycline Chase of the H2B-GFP/K5tTA Mouse to Visualize Label Dilution in the Fastest Cycling Epithelial Cells of the Eyelid Meibomian Glands

Eyelid meibomian glands are encircled by white lines.

(A and E) At 28-day pulse (no doxycycline), all nuclei of the meibomian gland epithelia are GFP$^+$.

(B and F) After 9-day chase, a few acini are diluted of GFP (red arrowheads), confirming that the fastest cycling cells of the meibomian gland are in the lipid-producing acini.

(C and G) A 13-day chase suggests that the ductal epithelium retains label stronger and cycles slower than the acini. Some acini have entirely diluted GFP (red arrowhead), whereas others have not significantly diluted GFP (white arrowhead), which suggests that their turnover is independently regulated.

(D and H) At 16-day doxycycline chase, acini have entirely diluted GFP label compared with the meibomian gland ductal epithelium.

putative adult stem cells were localized in whole mouse meibomian glands by pulse-chase labeling of LRCs (Figure 2). At 9 days post doxycycline, the duct and the majority of acini remain strongly labeled with GFP and label dilution appears unevenly distributed across the gland (Figure 2A). After 28-day chase, acini are significantly diluted of GFP fluorescence with the exception of a small subpopulation of LRCs confined to the terminal regions of the ductal epithelium within an acinus (Figures 2B, 2E, and 2F). While LRCs are located at the terminal ends of the ductal epithelium at the entrance to an acinus, not all acini contain detectable LRCs by 42-day doxycycline chase,

as observed in the 3D reconstructions of the whole meibomian gland (Figures 2C and 2G). The frequency of LRCs decreases from 28-day to 56-day chase (Figures 2D and 2H), and their decreasing number over time suggests that they remain functionally active while cycling at a remarkably slow rate.

After 3D reconstruction of DAPI and GFP signals in H2B-GFP/K5tTA mouse eyelids, we performed sequential immunostaining at 56-day doxycycline chase to characterize LRC differentiation and their proximity to K6$^+$ ductal epithelium (Figure 3). All GFP$^+$ slow-cycling cells were negative for the meibocyte differentiation marker PPAR-γ,
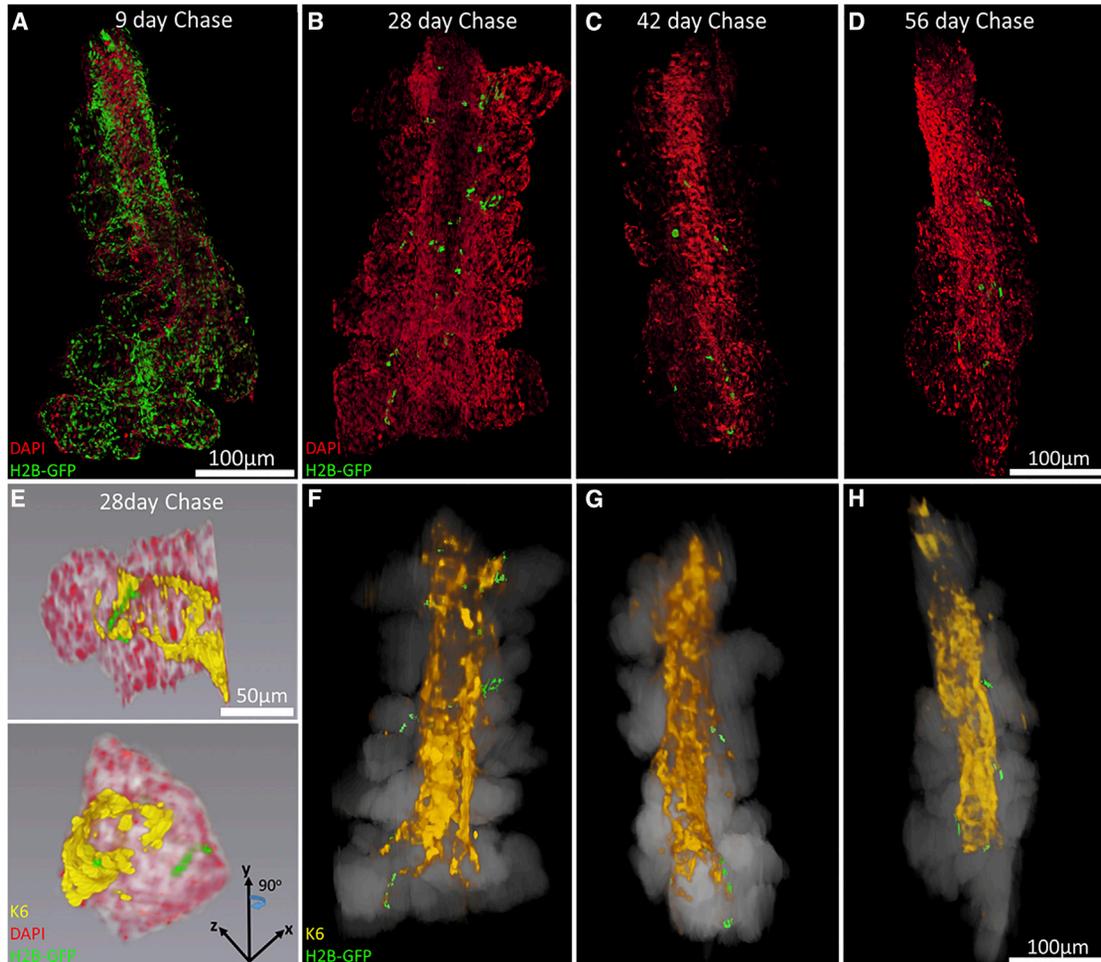
Figure 2. Immunofluorescent Tomography 3D Reconstructions of the H2B-GFP/K5tTA Mouse Meibomian Gland after Pulse-Chase

(A) Nine-day, (B and F) 28-day, (C and G) 42-day, and (D and H) 56-day doxycycline chase time points were 3D reconstructed using fluorescence signals from GFP$^+$ cells (green), K6$^+$ immunostained ductal epithelia (yellow), and DAPI-stained cell nuclei (red). LRCs were observed at the terminal ends of the K6$^+$ ductal epithelium at an entrance to an acinus.

(E) A close-up observation of an acini from a meibomian gland of an H2B-GFP/K5tTA mouse in 3D localized LRCs to the terminal ends of the K6$^+$ ductal epithelium where the ductule extends into an acinus.

confirming their undifferentiated state at 56-day chase (Figure 3A, yellow arrowhead). K6$^+$ staining confirmed that LRCs are localized to the terminal ends of the ductal epithelium, or the ductule leading to the acinar epithelium (Figure 3B). LRCs maintain K5 expression, like all meibomian gland epithelia (Figure 3C); however, K6 expression varied in LRCs (Figures 3E–3H), suggesting there may be two subpopulations of LRCs. To characterize K6 expression in LRCs, we quantified the K6$^+$ and K6$^-$ LRCs in the meibomian gland at 28-day (GFP$^+$/K6$^-$ = 20 ± 3; GFP$^+$/K6$^+$ = 6 ± 1), 42-day (GFP$^+$/K6$^-$ = 11 ± 1; GFP$^+$/K6$^+$ = 2 ± 0), and 56-day (GFP$^+$/K6$^-$ = 9 ± 2; GFP$^+$/K6$^+$ = 2 ± 0) doxycycline chase and found that the K6$^-$ LRC subpopulation retains label stronger than the K6$^+$ LRCs over longer chase time points.

LRC Fluorescence Intensity Variation and Keratin 14-Confetti Lineage Tracing of Epithelial Progenitors

Based on their average GFP fluorescence intensity in the meibomian gland of experimental H2B-GFP/K5tTA mice, relatively GFP-weak LRC populations were the majority in the meibomian gland (Figures 4A and 4B). We calculated that there was an average of 1 ± 1 LRC^{+++}, 3 ± 1 LRC^{++}, and 10 ± 2 LRC$^+$ subpopulations in the meibomian glands quantified at 42-day chase (n = 3). Vibrissae hair follicle LRC intensities at 42-day doxycycline chase (n = 3) were quantified as 18 ± 3 LRC^{+++}, 29 ± 5 LRC^{++}, and 37 ± 3 LRC$^+$ subpopulations. Therefore, meibomian gland LRCs are considerably faster cycling than the hair follicle LRCs (Figures 4C and 4D), which retain label more strongly and are greater in number at 42-day doxycycline
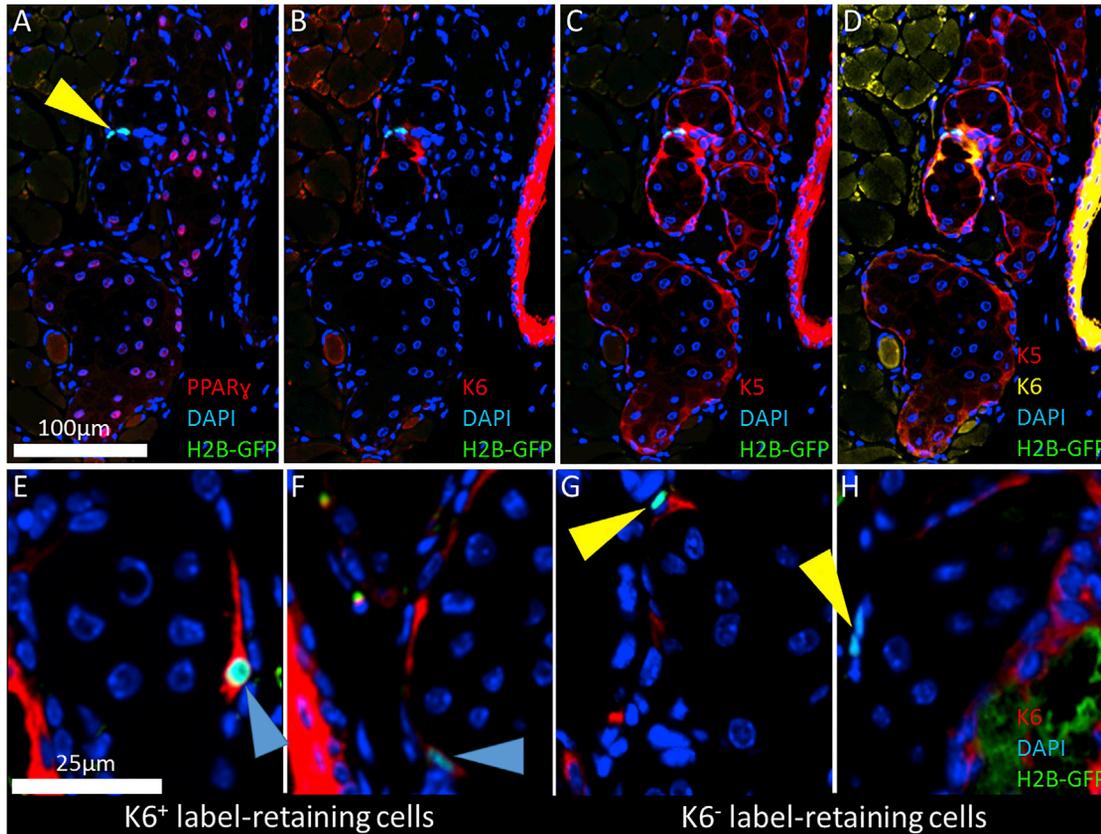
Figure 3. Immunohistochemistry Staining of the H2B-GFP/K5tTA Mouse Meibomian Gland LRCs at 56-Day Doxycycline Chase

(A) PPAR-γ was immunolabeled to identify lipid-producing meibocytes and confirm that LRCs (yellow arrowhead) are undifferentiated.

(B and C) K6 immunostaining co-localized LRCs with the terminal ends of the ductal epithelium (B) while K5 was found expressed in the entire meibomian gland epithelium (C).

(D) The overlay illustrates co-localization of K5+ and K6+ epithelial keratins in the meibomian gland and palpebral conjunctiva.

(E and F) A small subpopulation of LRCs were observed to express K6 (blue arrowhead), which indicated that a separate population of unipotent progenitors may exist to renew the duct.

(G and H) The majority of LRCs are K6− (yellow arrowhead).

chase. This variation in label dilution correlates with a variation in cell-cycle rate among LRCs and may point to a hierarchical mode of cell division in the meibomian gland.

We then used the K14CreER^T2-Confetti reporter line to evaluate lineage tracing of K14 epithelial progenitors and determined that individual acini are likely to arise from single progenitors separate from the precursor cells of ductal epithelium (Figure 5). This was confirmed in the 2-μm-thick butyl methyl methacrylate (BMMA) sections, where confetti-labeled meibomian gland acini were frequently monochromatic in color or not labeled (Figure 5A). The evidence for unipotent acini progenitors was also supported when K6 immunostaining was performed on a confetti-labeled acini and the duct was completely distinct from YFP labeling in the K14CreER^T2-Confetti mouse after a 23-week chase (Figure 5B). The labeling of entire acini in monochrome was analogous to the lineage-tracing pattern of K14 cells in the sebaceous gland, implying that each acinus in the gland arises from a single progenitor (Figure 5C). Fluorescence microscopy imaging of a 200-μm-thick vibratome section (Figure 5D) and 10-μm-thick cryosections (Figure 5E) showed that the ductal epithelium comprised multiple cell lineages, as contrasted by the monochromatic labeling of acini and the separate lineages of acini and duct at 23 weeks post tamoxifen injection in the K14CreER^T2-Confetti mouse.

At 59 weeks post tamoxifen injection of the K14CreER^T2-Confetti mouse, monochromatic and dual-labeled acini were also observed in the meibomian glands (Figure 6A). This further implies that individual acini originate from a single progenitor when two fluorescent proteins (RFP and GFP) are stochastically expressed and retained long term,
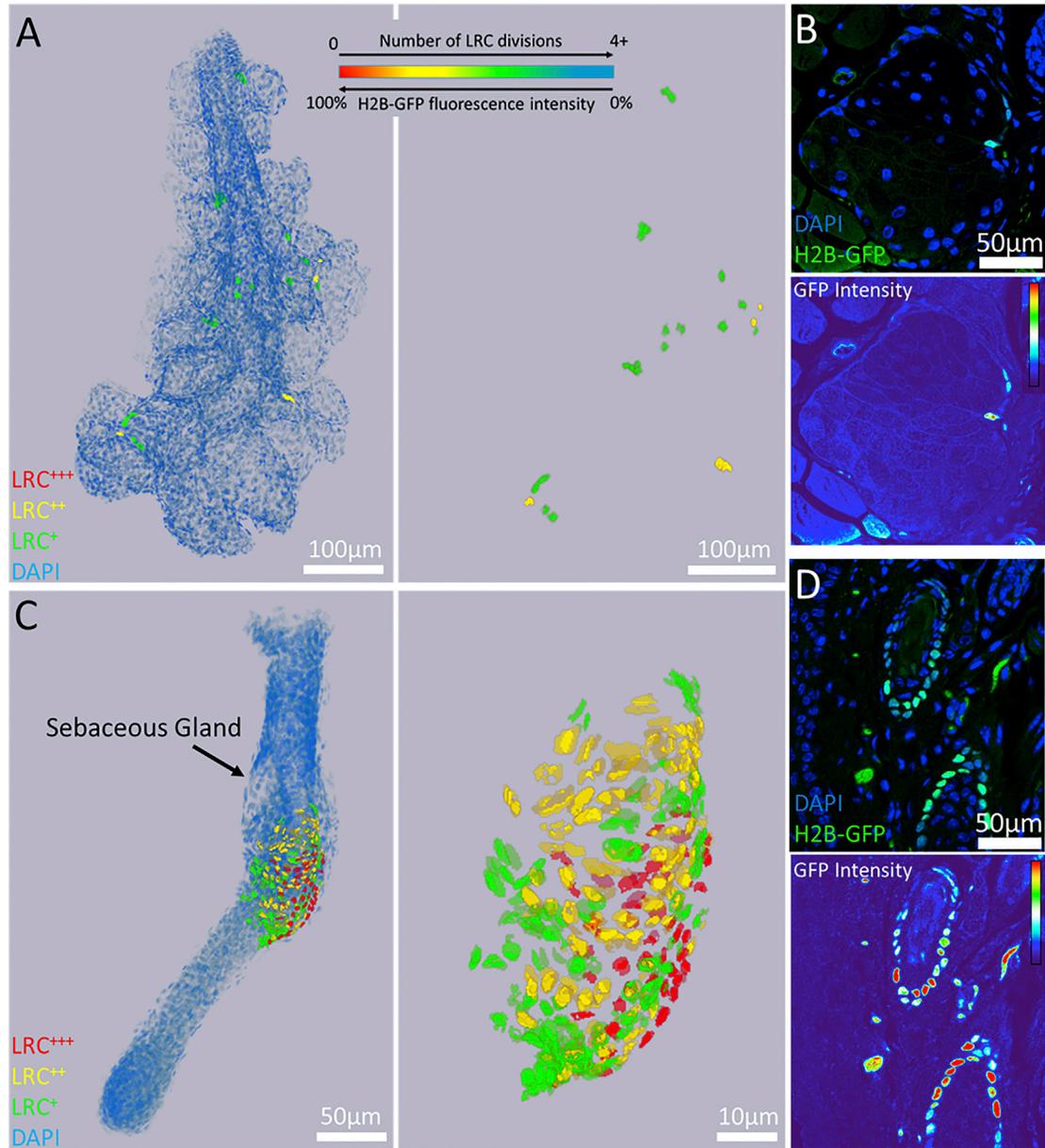
Figure 4. High-Resolution 3D Reconstructions of the Meibomian Gland and Vibrissae Hair Follicle Reveal a Gradient of Label Retention and GFP Fluorescence Intensity in LRCs at 42-Day Doxycycline Chase

(A and B) LRCs in the meibomian gland are relatively weak in fluorescence intensity when compared with (C and D) the vibrissae hair follicle, which has a larger range of GFP intensity and label retention in bulge LRCs. We quantified an average of 1 ± 1 LRC[+++], 3 ± 1 LRC[++], and 10 ± 2 LRC[+] subpopulations in the meibomian gland, and 18 ± 3 LRC[+++], 29 ± 5 LRC[++], and 37 ± 3 LRC[+] subpopulations in the vibrissae hair follicle at 42-day chase (n = 3).

59 weeks in this case. The 3D reconstruction generated by immunofluorescence tomography of the K14CreER[T2]-Confetti mouse meibomian gland (Figure 6B) also suggests that individual acini are derived from progenitor cells that renew the entire acini (Figure 6C), while the ductal epithelium is derived from multiple lineages separate from the acini (Figure 6D).

DISCUSSION

In this study, we characterized the epithelial cell-cycle differences across the murine meibomian gland, as well as the LRC subpopulations that we propose to be the progenitors responsible for the renewal of the meibomian gland. The variation in cell-cycle rate that we found between
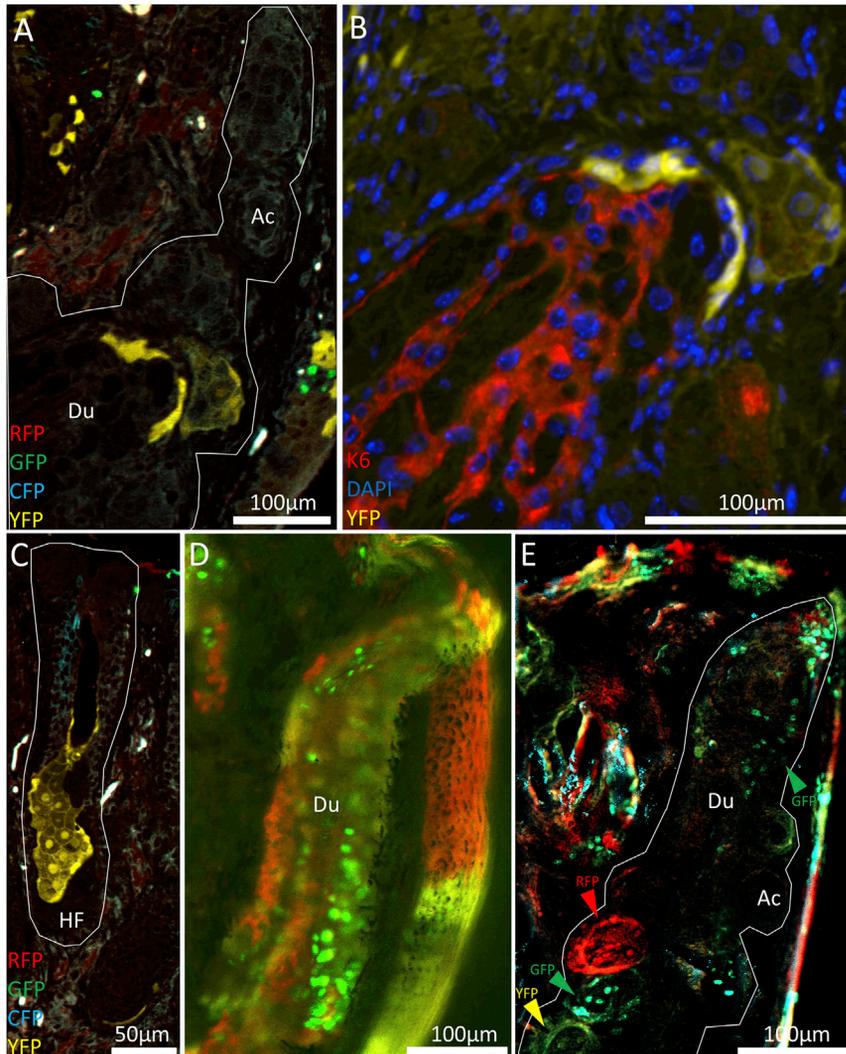
Figure 5. Lineage Tracing of K14$^+$ Epithelial Progenitors in the K14CreER^{T2}-Confetti Transgenic Mouse Meibomian Gland at 23 and 59 Weeks Post Tamoxifen Injection of a 10-Week-Old Mouse

(A) Individual acini are completely labeled with one color, suggesting that they are renewed from a single, independent lineage when compared with other acini and the ductal epithelium.

(B–E) K6 immunostaining confirms that acinar confetti labeling is separated from the ductal epithelium and suggests that there are distinct lineages for acini and ductal epithelium. Meibomian gland acinar labeling is analogous to the labeling of the sebaceous gland (C). Confetti labeling in a 200-μm vibratome section (D) and a 10-μm cryosection (E) also showed labeling in the ductal epithelium that is separate from the lineages stochastically labeled in the acini. Ac, acinus; Du, duct; HF, hair follicle.

each acinus, and between the acini and duct epithelium, suggests that they have distinct lineages that may operate on hierarchical cell-cycle programs. We used a lineage-tracing model to devise a hypothesis for cell turnover in the holocrine meibomian gland, in which unipotent LRCs renew individual acini and the ductal epithelium is derived from multiple, separate progenitor cells. In this way, the cell-cycle differences we observed between acini, and between acini and ductal epithelium, can be explained.

In the meibomian gland, low numbers of LRCs were observed after 28, 42, and 56 days of chase, which fulfill the slow-cycling, undifferentiated, and low population criteria of adult epithelial stem cells characterized in other tissues (Alonso and Fuchs, 2003; Stepp and Zieske, 2005; Tumbar et al., 2004). PPAR-γ immunostaining confirmed that the meibomian gland GFP$^+$ LRCs are undifferentiated and do not synthesize lipid, whereas differentiated meibo-

cytes undergoing lipogenesis enlarge and express nuclear PPAR-γ. The finding that meibomian gland LRCs retain label weaker and show greater reduction in numbers compared with the majority of hair follicle LRCs suggests that meibomian gland LRCs exist in lower populations and cycle faster than hair follicle LRCs in general. From this, we hypothesize that holocrine secretion and turnover of the meibomian gland epithelia is directed from quiescent LRCs located at the junction between ductal and acinar tissue (Figure 7). As these cells are typically found as clusters with varied levels of label retention, a hierarchical model of cell turnover in the meibomian gland can be considered whereby the slowest cycling LRC may represent the meibomian gland stem cell. However, there remains the possibility that meibocyte progenitors may exhibit neutral competition and divide stochastically to regenerate each acinus, as is the case for Lgr5 intestinal stem cells (Snippert et al., 2010).
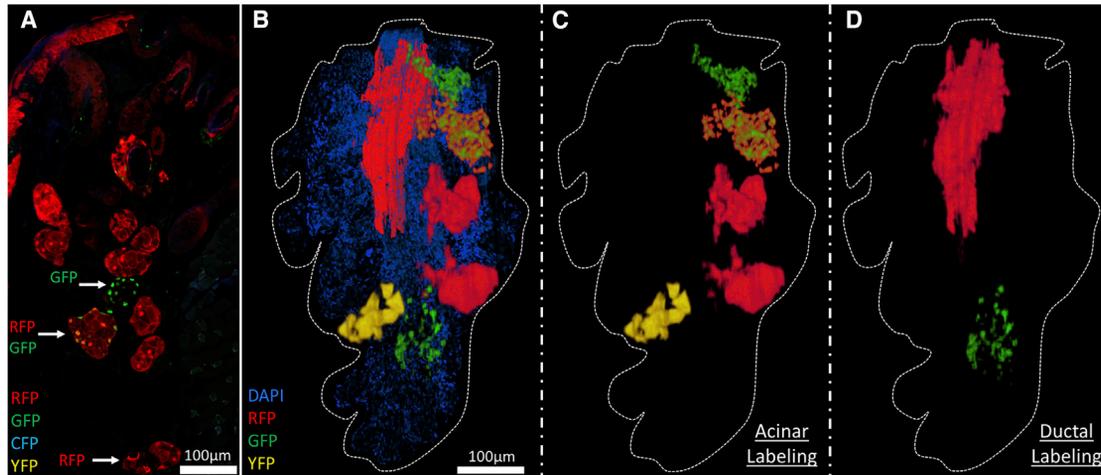
Figure 6. High-resolution 3D Reconstruction of the K14CreERT2-Confetti Mouse Eyelid after 59 Weeks Post Tamoxifen

(A) Fluorescence imaging of labels generated by stochastic recombination in the K14CreER^{T2}-Confetti mouse meibomian gland after 59 weeks verified that acini were entirely composed of a single color (RFP) or two-color combinations (RFP/GFP).

(B–D) A high-resolution 3D reconstruction of lineage tracing in the K14CreER^{T2}-Confetti mouse illustrates that (C) acini were independently labeled and (D) the duct comprised more than a single lineage. Dashed outlines encircle the entire meibomian gland structure.

Because of developmental similarities with skin appendages, and because they both secrete their contents in a holocrine manner, the meibomian gland is considered to be an enlarged, modified sebaceous gland and the mechanism of stem cell renewal is thought to show similar characteristics in these tissues (Knop et al., 2011). Epstein and Epstein (1966) originally showed that skin sebocytes differentiate over two distinct periods, i.e., between 7–9 days and 14–28 days, suggesting that migration and division of cells is heterogeneous in the peripheral basal layer (Epstein and Epstein, 1966), a finding supported by two distinct populations of sebocytes in the human forehead with different labeling indices (Plewig et al., 1971a, 1971b). Our short-term chase (<16 days) experiments in the H2B-GFP/K5tTA mouse meibomian gland revealed a variation in cell turnover between acini themselves, and between acini and ductal epithelium, suggesting that acini are not in synchrony across a single meibomian gland. In the K14CreER^{T2}-Confetti mouse, lineage tracing suggests that meibomian and sebaceous gland acini are derived from single-cell populations. When labeled, these acini are entirely composed of either one or two combined colors, which implies that renewal of an acinus comes from a single K14$^+$ progenitor cell. Lineage tracing in the 3D reconstructions also verified that transgenic fluorescent labels are limited to individual acini and do not label multiple acini or the ductal epithelium.

In the 3D reconstructions generated by immunofluorescence tomography of H2B-GFP/K5tTA mice at each doxycycline chase time point, quiescent LRCs were localized to the ductule region where K6$^+$ ductal epithelial cells terminate and the acini extend laterally. LRCs were observed to infrequently express K6, which indicates that two distinct unipotent LRC populations exist according to K6 expression. A unipotent progenitor giving rise to each acinus was supported by the lineage-tracing data, which show that acini are derived from a single progenitor cell over 59 weeks of long-term chase. If meibomian gland progenitors were bipotent, confetti labeling would extend from multiple acini into the ductal epithelium as a single progenitor renews both compartments of the gland, which was not observed herein. If LRCs are bipotent, the K6$^-$ LRC population is more likely to represent the adult stem cell population of the meibomian acinar population, as they are more label retaining than the K6$^+$ population after long-term pulse-chase. How these LRCs remain functional yet quiescent, and whether an extracellular stem cell niche exists underlying the meibomian gland basal layer that controls their quiescence and activation, still remains unclear.

Our data suggest that the region where the duct transitions into an acinus harbors the meibomian gland progenitors, and localized hyperproliferation previously reported in this region (Parfitt et al., 2013) could constitute a transiently amplifying cell population. From this, we propose that LRCs are unipotent, much like the limbal epithelial stem cells that exclusively renew cornea (Amitai-Lange et al., 2015; Collinson et al., 2002; Di Girolamo et al., 2015; Dora et al., 2015), and most likely exist in two populations that separately renew acinar or K6$^+$ ductal tissue. The heterogeneous nature of basal acinar cell divisions
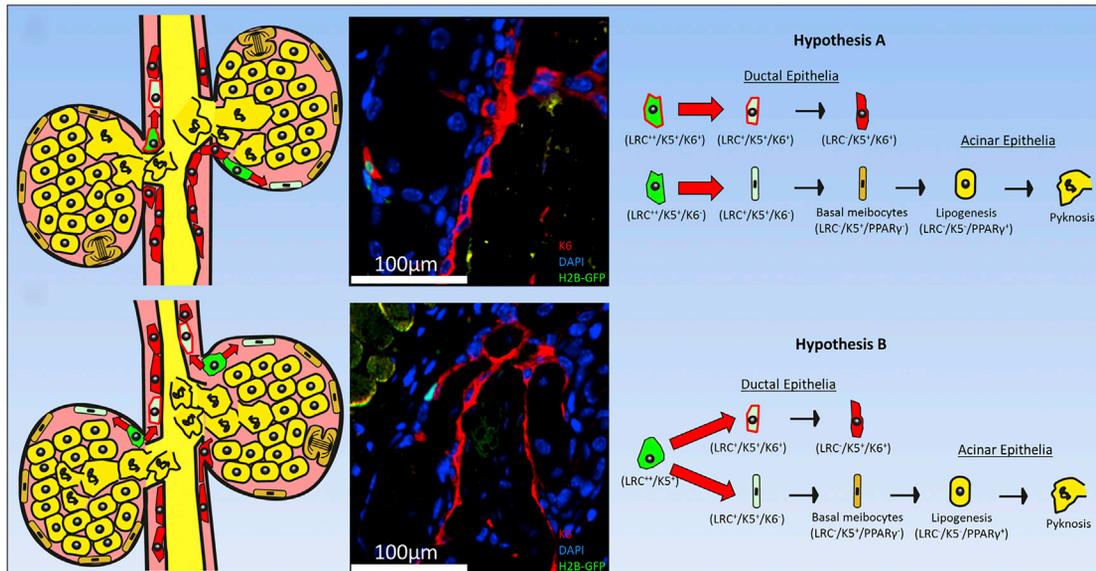
Figure 7. A New Hypothesis for Holocrine Turnover of the Meibomian Gland Maintained by Quiescent Progenitors Located at the Terminal Ends of the Ductal Epithelium

Adult meibomian gland acini are primarily composed of lipid-producing meibocytes (yellow) that have formed from basal acinar cells (dark green). Our data suggest that the terminal ends of the K6$^+$ ductal epithelium, or ductule, harbor the label-retaining progenitors (light green) that direct the renewal of acinar meibocytes (yellow) and ductal epithelium (red). In hypothesis A, LRCs are unipotent and capable of only renewing either acinar (K6$^-$) or ductal epithelial layers (K6$^+$). On the contrary, the K6$^+$ and K6$^-$ LRCs are derived from a bipotent LRC population that represents the adult stem cell of the meibomian gland, as in hypothesis B.

found previously (Epstein and Epstein, 1966; Plewig et al., 1971a, 1971b) may relate to LRCs in these terminal regions of the ductal epithelium that went undetectable in these studies. Finally, senescence of these LRC progenitors with age may be responsible for the meibomian gland atrophy and dry eye disease that are so prevalent with aging (Jester et al., 2011; Nien et al., 2009, 2011; Parfitt et al., 2013).

In conclusion, the meibomian gland contains a low population of slow-cycling epithelial cells that may constitute an adult stem cell population continually renewing the holocrine tissue. These LRCs vary in cell-cycle length according to label-retention differences in the H2B-GFP/K5tTA mouse after pulse-chase. Interestingly, acini within the same gland were found to dilute label at different rates over a short-term chase, which suggests that their cycle is independent. Gene-expression studies of these cells will provide more targets for further identification and isolation of LRCs, as well as insights into the gene regulation of LRC quiescence. However, transcriptional profiling of meibomian gland LRCs remains challenging because of their proximity to the hair follicle LRCs. In the future, the isolation of human meibomian gland adult stem cells could provide new regenerative therapies and fundamental insights into holocrine systems that are so vulnerable to age-related atrophy, particularly in dry eye disease.

EXPERIMENTAL PROCEDURES

H2B-GFP/K5tTA and K14CreERT2-Confetti Reporter Mouse Generation for Label Retention and Lineage Tracing of Epithelial Progenitors

K5tTA transgenic mice were generously provided by Stuart Yuspa at the National Cancer Institute (Diamond et al., 2000) while Tg(tetO-HIST1H2BJ/GFP)47Efu/J (H2B-GFP) transgenic mice were obtained from the Jackson Laboratory (005104) (Tumbar et al., 2004). Mice were genotyped in-house by PCR. K14CreER^{T2} mice were a kind gift from Daniel Metzger and Pierre Chambon (Indra et al., 2005).

H2B-GFP/K5tTA mice were pulse-labeled from postnatal day 0, when the meibomian gland develops from elongating epidermal invaginations (Nien et al., 2010), until doxycycline chase to turn off H2B-GFP expression at postnatal day 28. To validate that all meibomian gland cells were labeled prior to doxycycline chase, we euthanized mice at 28-day pulse and cross-sectioned their eyelids by cryosectioning at 10 μm. At 28-day pulse, H2B-GFP/K5tTA mice were fed 2 g/kg doxycycline chow (Bio-Serv) and three mice were each euthanized after the 9-, 13-, 16-, 28-, 42-, and 56-day chase time points to evaluate label dilution and meibocyte proliferation, and to replicate pulse-chase experiments performed to determine the location of quiescent corneal and epidermal stem cells (Cotsarelis et al., 1989; Tumbar et al., 2004).

K14CreER^{T2}-Confetti mice were pulsed with tamoxifen at 10 weeks of age as previously outlined (Di Girolamo et al., 2015) and euthanized at 33 and 69 weeks of age (23- and 59-week chase),

and excised tissue was fixed in 4% paraformaldehyde. The K14-driven confetti reporter mouse contains the Brainbow 2.1 fluorescent multicolor cassette with a *Cre* construct downstream of the keratin 14 promoter. *Cre* is fused to an estrogen receptor (ER) and is induced by tamoxifen before *Cre*ER translocates to the nucleus. The multicolor Brainbow 2.1 cassette construct is in two segments, each containing two fluorescent proteins in a sense/anti-sense orientation, which is inserted within the *Rosa26* locus. Flanking *loxP* sites of each segment enables *Cre* recombination, and each color generated is dependent on the orientation and sequence inserted back into the *Rosa26* locus after excision because of the opposite *loxP* sequences. As recombination is stochastic, there are ten possible fluorescence outcomes in homozygous Confetti cells and each label is localized to a different cellular compartment; CFP is expressed in the membrane whereas GFP is nuclear and YFP and RFP are cytoplasmic.

Animals were treated according to the ARVO statement on the use of animals in vision research, and experiments with the H2B-GFP/K5tTA mice were approved by the IACUC of the University of California, Irvine (P.I. Jester, protocol # 2011-3002, approved September 8, 2011). Studies with K14CreER^T2-Confetti mice were performed according to the Australian Code of Practice for the Care and Use of Animals for Scientific Purposes, which were also approved by the University of New South Wales' Animal Ethics Committee (14/89). Mice were euthanized through carbon dioxide asphyxiation and cervical dislocation at each time point. Then fixed eyelids were embedded in low-melting-point 3% agarose to orient the tissue correctly for BMMA plastic embedding and serial sectioning. Tissues were then ethanol (EtOH) dehydrated in increasing concentrations of EtOH (50%–75%–90%–100% at 30-min intervals before BMMA resin infiltration with incremental concentrations of 2:1, 1:1, and 1:2 EtOH/BMMA). BMMA-embedded blocks were then polymerized for a minimum of 8 hr using UV light at 4°C.

Serial Sectioning and Immunostaining

For each chase time point of the label-retaining and lineage-tracing mouse models, eyelid tissues were 3D reconstructed from three individual H2B-GFP/K5tTA bigenic (28-, 42-, and 56-day chase [n = 9]) and K14CreER^T2-Confetti (23- and 59-week chase [n = 6]) transgenic mice. Meibomian glands embedded in BMMA were serially sectioned at 2 μm using a Leica ultra-microtome equipped with a diamond knife (DiAtome). After sectioning, plastic sections were spread out using chloroform to remove cutting compression, and ribbons of serial sections were obtained when Pattex glue (Henkel) was added to the block edge before sectioning. The protocol for sequential immunostaining and mosaic imaging of serial sections for immunofluorescence tomography has been previously published (Parfitt et al., 2012).

Sections were initially treated with acetone for 10 min to remove BMMA plastic and mounted with 1:1 glycerol/PBS with 1:15,000 DAPI (1 mg/ml) before image acquisition. DAPI-stained nuclei were used to overlay and align the GFP images with corresponding immunofluorescence images. After imaging GFP fluorescence, serial sections were sequentially immunolabeled with Keratin 6 (Ab24646, Abcam), Keratin 5 (Ab53121, Abcam), and PPAR-γ (2435S, Cell Signaling Technology) to identify ductal epithelium and markers of meibocyte differentiation, respectively. In the K14CreER^T2-Confetti mice, endogenous RFP was quenched during the BMMA polymerization process by EtOH dehydration and was recovered before imaging using an antibody to RFP (DPATB-H83194, Creative Diagnostics).

For immunostaining of BMMA plastic serial sections, tissues were rehydrated in 95%, 75%, and 50% EtOH/PBS for 10-min intervals and then 1× PBS for 5 min before antigen retrieval and sequential immunostaining in a Ted Pella Biowave (Ted Pella) as previously described (Parfitt et al., 2012, 2013). Once immunostained, cell nuclei were fluorescently labeled with DAPI to aid the semi-automated alignment of serial sections. For fluorescence microscopy using a Zeiss LSM 510, cryosections of tissue embedded with optimal cutting temperature compound were cut at 10 μm on a Leica cryostat while vibratome sections of 10% agarose-embedded tissue were cut at 200 μm.

Electron Microscopy, Fluorescence Microscopy, and 3D Reconstruction of LRC Subpopulations

Transmission electron microscopy of 100-nm BMMA-embedded eyelid sections was performed on a JEOL 1010 microscope, after staining grids with saturated aqueous uranyl acetate and 1% aqueous phosphotungstic acid for contrast enhancement of collagen. Prior to immunofluorescence staining and fluorescence microscopy, GFP fluorescence was imaged in the H2B-GFP/K5tTA mouse eyelid 2-μm BMMA serial sections to preserve signal. Imaging of K14CreER^T2-Confetti mice serial sections was carried out using a Zeiss LSM 510 multi-photon microscope to excite the multiple fluorophores across the four wavelengths (CFP, GFP, YFP, RFP). CFP was excited at 435 nm and its emission collected at 485 nm, whereas GFP was excited at 488 nm and collected at 510 nm; YFP was excited at 517 nm and its emission collected at 530 nm; and RFP was excited at 543 nm and the emission collected at 560 nm.

Imaging of GFP fluorescence and antibody markers in serial sections from H2B-GFP/K5tTA mice was carried out using a Leica DMI6000B inverted epifluorescence microscope (Leica) with an ASI automated stage driven by Metamorph software (Molecular Devices). Mosaic imaging of multiple fluorophores with specific excitation and emission wavelengths was carried out using a Zeiss 510 LSM microscope. Sections were individually imaged in a 3 × 4 mosaic using a 20× 0.75NA objective and with a pixel area of 0.44 μm^2. Ten-percent stitching of mosaics was completed using ImageJ. The stitched mosaics which make up the image of each section were converted to 8 bits before semi-automated alignment and segmentation using Amira software (Visage Imaging). The average pixel intensities of GFP$^+$ LRCs was calculated using Amira segmentation and each LRC was assigned into a category based on their intensity value and level of label retention, with the LRC^{+++} subpopulation being the most quiescent (i.e., LRC$^+$ = 0–100; LRC^{++} = 100–200; LRC^{+++} = 200–255).

REFERENCES

Alonso, L., and Fuchs, E. (2003). Stem cells of the skin epithelium. Proc. Natl. Acad. Sci. USA *100* (*Suppl 1*), 11830–11835.

Amitai-Lange, A., Altshuler, A., Bubley, J., Dbayat, N., Tiosano, B., and Shalom-Feuerstein, R. (2015). Lineage tracing of stem and progenitor cells of the murine corneal epithelium. Stem Cells *33*, 230–239.

Barker, N., van Es, J.H., Kuipers, J., Kujala, P., van den Born, M., Cozijnsen, M., Haegebarth, A., Korving, J., Begthel, H., Peters, P.J., et al. (2007). Identification of stem cells in small intestine and colon by marker gene Lgr5. Nature *449*, 1003–1007.

Blanpain, C., and Fuchs, E. (2006). Epidermal stem cells of the skin. Annu. Rev. Cell Dev. Biol. *22*, 339–373.

Call, M., Fischesser, K., Lunn, M.O., and Kao, W.W. (2016). A unique lineage gives rise to the meibomian gland. Mol. Vis. *22*, 168–176.

Chen, W., Ishikawa, M., Yamaki, K., and Sakuragi, S. (2003). Wistar rat palpebral conjunctiva contains more slow-cycling stem cells that have larger proliferative capacity: implication for conjunctival epithelial homeostasis. Jpn. J. Ophthalmol. *47*, 119–128.

Collinson, J.M., Morris, L., Reid, A.I., Ramaesh, T., Keighren, M.A., Flockhart, J.H., Hill, R.E., Tan, S.S., Ramaesh, K., Dhillon, B., et al. (2002). Clonal analysis of patterns of growth, stem cell activity, and cell movement during the development and maintenance of the murine corneal epithelium. Dev. Dyn. *224*, 432–440.

Cotsarelis, G., Cheng, S.Z., Dong, G., Sun, T.T., and Lavker, R.M. (1989). Existence of slow-cycling limbal epithelial basal cells that can be preferentially stimulated to proliferate: implications on epithelial stem cells. Cell *57*, 201–209.

Cotsarelis, G., Sun, T.T., and Lavker, R.M. (1990). Label-retaining cells reside in the bulge area of pilosebaceous unit: implications for follicular stem cells, hair cycle, and skin carcinogenesis. Cell *61*, 1329–1337.

Diamond, I., Owolabi, T., Marco, M., Lam, C., and Glick, A. (2000). Conditional gene expression in the epidermis of transgenic mice using the tetracycline-regulated transactivators tTA and rTA linked to the keratin 5 promoter. J. Invest. Dermatol. *115*, 788–794.

Dora, N.J., Hill, R.E., Collinson, J.M., and West, J.D. (2015). Lineage tracing in the adult mouse corneal epithelium supports the limbal epithelial stem cell hypothesis with intermittent periods of stem cell quiescence. Stem Cell Res. *15*, 665–677.

Duque, A., and Rakic, P. (2011). Different effects of bromodeoxyuridine and [^{3}H]thymidine incorporation into DNA on cell proliferation, position, and fate. J. Neurosci. *31*, 15205–15217.

Epstein, E.H., Jr., and Epstein, W.L. (1966). New cell formation in human sebaceous glands. J. Invest. Dermatol. *46*, 453–458.

Fuchs, E., and Horsley, V. (2011). Ferreting out stem cells from their niches. Nat. Cell Biol. *13*, 513–518.

Fuchs, E., and Segre, J.A. (2000). Stem cells: a new lease on life. Cell *100*, 143–155.

Di Girolamo, N., Bobba, S., Raviraj, V., Delic, N.C., Slapetova, I., Nicovich, P.R., Halliday, G.M., Wakefield, D., Whan, R., and Lyons, J.G. (2015). Tracing the fate of limbal epithelial progenitor cells in the murine cornea. Stem Cells *33*, 157–169.

Horwath-Winter, J., Berghold, A., Schmut, O., Floegel, I., Solhdju, V., Bodner, E., Schwantzer, G., and Haller-Schober, E.M. (2003). Evaluation of the clinical course of dry eye syndrome. Arch. Ophthalmol. *121*, 1364–1368.

Indra, A.K., Dupe, V., Bornert, J.M., Messaddeq, N., Yaniv, M., Mark, M., Chambon, P., and Metzger, D. (2005). Temporally controlled targeted somatic mutagenesis in embryonic surface ectoderm and fetal epidermal keratinocytes unveils two distinct developmental functions of BRG1 in limb morphogenesis and skin barrier formation. Development *132*, 4533–4544.

Jester, B.E., Nien, C.J., Winkler, M., Brown, D.J., and Jester, J.V. (2011). Volumetric reconstruction of the mouse meibomian gland using high-resolution nonlinear optical imaging. Anat. Rec. (Hoboken) *294*, 185–192.

Knop, E., Knop, N., Millar, T., Obata, H., and Sullivan, D.A. (2011). The international workshop on meibomian gland dysfunction: report of the subcommittee on anatomy, physiology, and pathophysiology of the meibomian gland. Invest. Ophthalmol. Vis. Sci. *52*, 1938–1978.

Lavker, R.M., Treet, J., and Su, T. (2003). Label-retaining cells (LRCs) are preferentially located in the ductal epithelium of the meibomian gland: implications on the mucocutaneous junctional (MCJ) epithelium of the eyelid. IOVS *44*, ARVO e-abstract 3781.

Lavker, R.M., and Sun, T.T. (1983). Epidermal stem cells. J. Invest. Dermatol. *81*, 121s–127s.

Lavker, R.M., Tseng, S.C., and Sun, T.T. (2004). Corneal epithelial stem cells at the limbus: looking at some old problems from a new angle. Exp. Eye Res. *78*, 433–446.

Lemp, M.A., Crews, L.A., Bron, A.J., Foulks, G.N., and Sullivan, B.D. (2012). Distribution of aqueous-deficient and evaporative dry eye in a clinic-based patient cohort: a retrospective study. Cornea *31*, 472–478.

Nadri, S., Soleimani, M., Kiani, J., Atashi, A., and Izadpanah, R. (2008). Multipotent mesenchymal stem cells from adult human eye conjunctiva stromal cells. Differentiation *76*, 223–231.

Nagasaki, T., and Zhao, J. (2005). Uniform distribution of epithelial stem cells in the bulbar conjunctiva. Invest. Ophthalmol. Vis. Sci. *46*, 126–132.

Nien, C.J., Paugh, J.R., Massei, S., Wahlert, A.J., Kao, W.W., and Jester, J.V. (2009). Age-related changes in the meibomian gland. Exp. Eye Res. *89*, 1021–1027.

Nien, C.J., Massei, S., Lin, G., Liu, H., Paugh, J.R., Liu, C.Y., Kao, W.W., Brown, D.J., and Jester, J.V. (2010). The development of meibomian glands in mice. Mol. Vis. *16*, 1132–1140.

Nien, C.J., Massei, S., Lin, G., Nabavi, C., Tao, J., Brown, D.J., Paugh, J.R., and Jester, J.V. (2011). Effects of age and dysfunction on human meibomian glands. Arch. Ophthalmol. *129*, 462–469.

Olami, Y., Zajicek, G., Cogan, M., Gnessin, H., and Pe'er, J. (2001). Turnover and migration of meibomian gland cells in rats' eyelids. Ophthalmic Res. *33*, 170–175.

Parfitt, G.J., Xie, Y., Reid, K.M., Dervillez, X., Brown, D.J., and Jester, J.V. (2012). A novel immunofluorescent computed tomography (ICT) method to localise and quantify multiple antigens in large tissue volumes at high resolution. PLoS One *7*, e53245.

Parfitt, G.J., Xie, Y., Geyfman, M., Brown, D.J., and Jester, J.V. (2013). Absence of ductal hyper-keratinization in mouse age-related meibomian gland dysfunction (ARMGD). Aging *5*, 825–834.

Parfitt, G.J., Geyfman, M., Xie, Y., and Jester, J.V. (2015). Characterization of quiescent epithelial cells in mouse meibomian glands and hair follicle/sebaceous glands by immunofluorescence tomography. J. Invest. Dermatol. *135*, 1175–1177.

Pinto, D., and Clevers, H. (2005). Wnt, stem cells and cancer in the intestine. Biol. Cell *97*, 185–196.

Plewig, G., Christophers, E., and Braun-Falco, O. (1971a). Cell transition in human sebaceous glands. Acta Derm. Venereol. *51*, 423–428.

Plewig, G., Christophers, E., and Braun-Falco, O. (1971b). Proliferative cells in the human sebaceous gland. Labelling index and regional variations. Acta Derm. Venereol. *51*, 413–422.

Rinkevich, Y., Lindau, P., Ueno, H., Longaker, M.T., and Weissman, I.L. (2011). Germ-layer and lineage-restricted stem/progenitors regenerate the mouse digit tip. Nature *476*, 409–413.

Snippert, H.J., van der Flier, L.G., Sato, T., van Es, J.H., van den Born, M., Kroon-Veenboer, C., Barker, N., Klein, A.M., van Rhee-nen, J., Simons, B.D., et al. (2010). Intestinal crypt homeostasis results from neutral competition between symmetrically dividing Lgr5 stem cells. Cell *143*, 134–144.

Stepp, M.A., and Zieske, J.D. (2005). The corneal epithelial stem cell niche. Ocul. Surf. *3*, 15–26.

Su, L., Cui, H., Xu, C., Xie, X., Chen, Q., and Gao, X. (2011). Putative rabbit conjunctival epithelial stem/progenitor cells preferentially reside in palpebral conjunctiva. Curr. Eye Res. *36*, 797–803.

Suhalim, J.L., Parfitt, G.J., Xie, Y., De Paiva, C.S., Pflugfelder, S.C., Shah, T.N., Potma, E.O., Brown, D.J., and Jester, J.V. (2014). Effect of desiccating stress on mouse meibomian gland function. Ocul. Surf. *12*, 59–68.

Sun, T.T., Cotsarelis, G., and Lavker, R.M. (1991). Hair follicular stem cells: the bulge-activation hypothesis. J. Invest. Dermatol. *96*, 77S–78S.

Tumbar, T., Guasch, G., Greco, V., Blanpain, C., Lowry, W.E., Rendl, M., and Fuchs, E. (2004). Defining the epithelial stem cell niche in skin. Science *303*, 359–363.

Vascotto, S.G., and Griffith, M. (2006). Localization of candidate stem and progenitor cell markers within the human cornea, limbus, and bulbar conjunctiva in vivo and in cell culture. Anat. Rec. A Discov. Mol. Cell. Evol. Biol. *288*, 921–931.

You, S., Tariq, A., Kublin, C.L., and Zoukhri, D. (2011). Detection of BrdU-label retaining cells in the lacrimal gland: implications for tissue repair. Cell Tissue Res. *346*, 317–326.